Analele Universităţii de Vest din Timişoara
Vol. XLVII, 2006
Seria Fizică

DYNAMICAL PROPERTIES OF METAL CLUSTERS

C. Lupulescu, L. D. Socaciu-Siebert, E. C. Stanca-Kaposta, A. Merli and L. Wöste

Institut für Experimentalphysik, Freie Universität Berlin, Arnimallee 14, D-14195, Berlin, Germany

Abstract
Acest articol prezintă o serie de metode experimentale aplicate in scopul studierii proprietaţilor statice şi dinamice ale clusterilor metalici. Proprietăţile catalitice ale aurului au fost demonstrate folosind cinetica reacţiilor chimice. Spectroscopia in infraroşu susţinută de calcule teoretice a fost aplicată in cazul oxizilor de vanadiu pentru a cunoaşte structura moleculară ce determină reactivitatea catalizatorilor. Caracterul dinamic al clusterilor metalici a fost investigat folosind spectroscopia cu rezoluţie temporală ultrascurtă. Metoda controlului coerent a permis influenţarea şi descifrarea mecanismelor reacţiilor fotochimice.
Keywords: reactivity, infrared spectroscopy, coherent control.

1. Introduction

Although the catalytic properties of nanoscale particles were intensively studied during the past decades, the intrinsic mechanisms of the heterogenous catalysis and reaction dynamics at atomic and molecular level are still unknown. Model systems which have similar properties to the real catalysts and are also theoretically accessible were needed. In this context, clusters consisting of a few atoms up to a few thousands of atoms are good conceptual systems to study elementary mechanisms of heterogeneous catalysis and reaction dynamics. In this non-scalable regime the electronic structure still has a discrete, quantified character and thus, every cluster with a specific number of atoms and electrons has its own intrinsic, characteristic electronic structure. Due to this feature, by adding or removing a single atom from a cluster of a certain size, drastic changes in the physical and chemical properties can be obtained. A better understanding of the activity of these small systems in chemical processes can be gained by using coherent control schemes. In these experiments the shape (i.e. phase- and/or amplitude) of a femtosecond (fs) laser pulse is actively modified in order to drive a reaction towards a maximum yield. The experiment does not only learn to control the dynamics of a cluster, but also acquires information about wavepacket propagation on potential energy surfaces of the involved system.
In this manuscript we present a brief overview of our results on dynamic properties of clusters. The first describe the reaction kinetics and fs-dynamics of gold, silver and Ag_2O_2 clusters. The

determination of cluster's structure using infrared photodissociation spectroscopy is illustrated in the second part on vanadium oxide cations. Finally, an example of a coherent control experiment applied on the combined multi-photon ionization of NaK and fragmentation from Na_2K is presented.

2. Reaction kinetics and femtosecond dynamics on noble metal clusters

Until quite recently gold and silver have not been considered relevant for the design of new materials for heterogeneous catalysis, because of their inert nature. However, when the particle size is reduced to the nanometer range, gold and silver loose their nobleness and exbit a striking reactive behaviour [1]. During the past few years new catalysts based on highly dispersed nano-scale gold particles were developed [2-3]. Most recently, it was found that mass-selected deposited gold clusters Au_n^- ($n \geq 8$) on thin films of MgO(100) catalyze the CO oxidation reaction [4]. Due to this, the efforts were focused on the study of the catalytic properties of small, gas-phase, mass-selected, charged gold and silver clusters towards the oxidation reaction of carbon monoxide. We performed experiments in which mass-selected Au_n^- ($n \leq 3$) and Ag_n^- ($n \leq 11$) cluster ions are exposed to a CO/O_2/He gas mixture inside an rf-octopole ion trap at a defined reaction temperature. The experimental setup consists of an octopole ion trap inserted into a tandem quadrupole mass spectrometer arrangement: the cluster anions are produced by a CORDIS ion source, mass-selected with a first quadrupole mass filter and transferred into a temperature variable radio frequency (rf)-octopole ion trap. The octopole ion trap is pre-filled with about 1 Pa partial pressure of He buffer gas and a small, well defined fraction of reactive gases (CO and O_2). The ion trap is attached to a helium cryostat allowing variable temperature adjustment in the range between 20 K and 350 K. Details to the experimental apparatus can be found in [5]. The cluster ions are stored inside the trap (reaction time t_R) up to ten seconds without significant ion loss. After the chosen reaction time all ions, reactants, intermediates, and products, are extracted and the ion distribution is analyzed via a second quadrupole mass spectrometer. With this experimental arrangement mass spectra and reaction kinetics can be measured, i.e. by recording all ion concentrations as a function of the reaction time the kinetics of the reaction is obtained. Possible reaction mechanisms are evaluated by fitting the integrated rate equations to the experimental kinetic data and thus, the reaction rate constants are obtained.

Fig. 1a and 1b (upper part) show the recorded mass-spectra for the reactions of Au_n^- ($n \leq 3$) and Ag_n^- ($n \leq 11$) anionic clusters with molecular oxygen [6-8]. Alternating size effects in the reactivity of noble metal anions towards O_2 can be observed: odd-numbered silver anions bind up to two O_2 molecules, whereas even-numbered silver anions bind only one O_2 molecule. In the case of gold clusters, only even-numbered anions can attach only one O_2 and no additional adsorption of oxygen molecules is observed. The binding mechanism of oxygen molecules is based on an electron transfer from the highest occupied molecular orbital of the

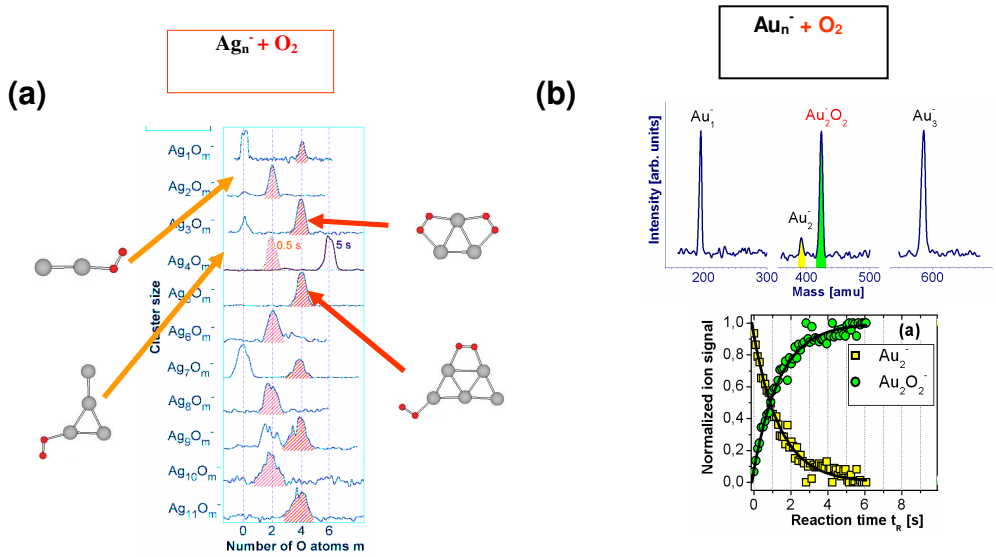

Fig.1 *Product ion mass spectra for the reaction of Ag_n^-(a) and Au_n^- (b) with O_2 . (a) The corresponding structures were calculated theoretically (big spheres: sliver atoms, small spheres: oxygen atoms). (b) The mass spectra Au_n^- with O_2 (upper part) and reaction kinetics of Au_2^- clusters with O_2 (lower part).*

cluster into one of the antibonding orbitals of the O_2 molecule. The structures of the $Ag_nO_m^-$ complexes were calculated in the framework of the density functional theory (DFT) in the group of Bonačić-Koutecký [7]. The odd-even effects in the reactivity of the negatively charged noble metal clusters with oxygen molecules can be correlated with the alternating vertical detachment energies (VDE) of the metal anions: clusters with a low value for VDE can donate more easily an electron to the oxygen ligand than negatively charged clusters, which present a higher value for the VDE and thus, show less or even no reactivity towards O_2. Fig. 1b (lower part) shows the kinetic traces of the reaction of Au_2^- with O_2.

In order to investigate the catalytic properties of Au_2- clusters towards the oxidation reaction of CO, the reactivity of anionic gold dimers with O_2 and CO was investigated. The

reaction kinetics as a function of O_2 /CO concentrations for a reaction temperature of 300 K are displayed in Fig. 2 [8]. The simplest reaction mechanism that is able to fit the experimental data is an equilibrium reaction where k_1 and k_{-1} are the rate constants for the forward and backward reactions, respectively.

$$Au_2^- + O_2 \underset{k_{-1}}{\overset{k_1}{\leftrightarrow}} Au_2O_2^-$$

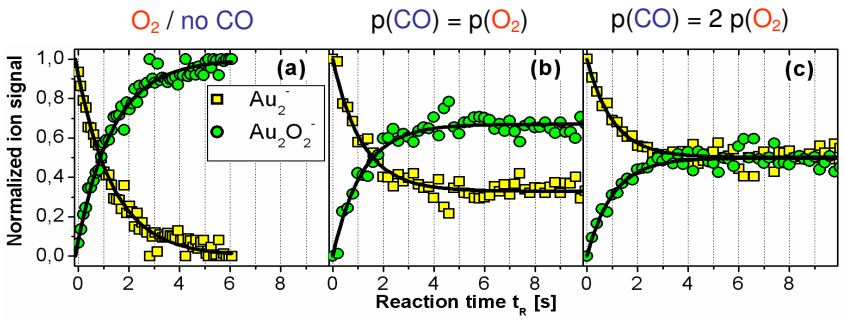

Fig.2 *Kinetic traces of all product ions observed during Au_2^- reaction with O_2 and CO inside the octopole ion trap as a function of the reaction time t_R for different CO partial pressures. The filled symbols represent the normalized experimental data and the solid lines are obtained by fitting the integrated rate equations of the proposed reaction mechanisms to the experimental data.*

It is important to note that the Au_2^- offset, i.e. the equilibrium concentration of Au_2^- is only observed when CO is present in the ion trap, although this is not reflected in the upper equation. Moreover, this offset increases with increasing CO partial pressure (Fig. 2b and 2c) and the backward reaction step k_{-1} is enhanced. Thus, the above indicates that the equation fails to provide a complete description of the reaction and that an appropriate description involves more complex reaction steps. In order to gain further insight into the mechanism of this reaction, the reaction products as a function of the reaction temperature were recorded. Fig. 3 shows a mass spectrum of the production distribution under room-temperature conditions with both reactive gases present in the trap. At 300 K only Au_2^- and $Au_2O_2^-$ are detected. Surprisingly, cooling the ion trap down below room temperature (100 K) revealed the appearance of an additional signal (Fig. 3a). The new ion signal emerges at the mass assigned to the species with a stoichiometry of $Au_2(CO)O_2^-$. The formation of $Au_2(CO)O_2^-$ as final reaction product clearly shows that Au_2^- favours the co-adsorption of both, O_2 and CO, over the adsorption of just one type of reactive molecule. The theoretical calculations based on DFT are performed by H. Häkkinen and U. Landman [8]. Many isomeric structures can be assigned for the co-adsorption complex with the

mass corresponding to $Au_2(CO)O_2^-$. The two extreme cases are: the $Au_2(CO)O_2^-$ structure, which is formed when the CO and O_2 molecules are adsorbed independently, for example on different sides of Au_2^- and the $Au_2(CO_3)^-$ structure, which is formed when a reaction of the two adsorbate molecules takes place, resulting in a carbonate (CO_3) entity. It is important to note that the product $Au_2(CO_3)^-$ has been proposed theoretically [9] to be a key intermediate in a catalytic CO oxidation cycle on Au_2^- clusters. The peroxyformate-like species $Au_2(CO)O_2^-$ where the O-O bond is elongated compared to the gas-phase oxygen molecule can be formed without an activation barrier and is assumed to be able to redesorb CO as observed in the experiment. Both, the peroxyformate-like species $Au_2(CO)O_2^-$ and carbonate species $Au_2(CO_3)^-$ have low activation barriers for the formation of CO_2 and thus facilitating the observed low-temperature catalytic activity of Au_2^-.

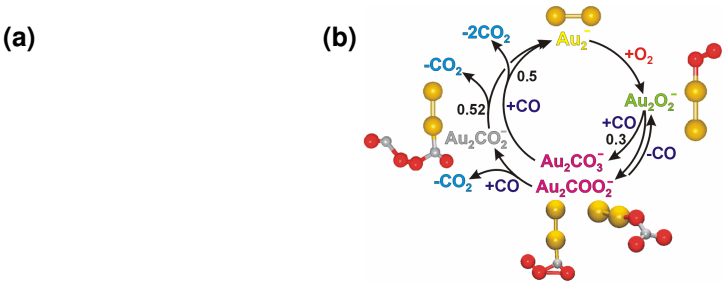

Fig. 3 *a) Mass spectra of product ion distributions for the reaction of Au_2^- with O_2 and CO. b): The complete gas-phase catalytic cycle of gold dimer anions for the oxidation CO, based on the reaction mechanism determined by kinetic measurements in conjunction with first-principles calculation [8].*

Additional information about the fs-dynamics of a reaction educts or products can be obtained by employing the NeNePo spectroscopy. This pump-probe negative ion-to-neutral-to-positive (NeNePo) technique, developed in our group, allows for the study of the nuclear dynamics of a system on the neutral potential energy surface of the electronic ground state and it was successfully applied to the study of the fs-dynamics of noble metal clusters [10]. The principle of the NeNePo-spectroscopy is depicted in Fig. 4a: the experiment starts with the production of an anionic cluster ensemble. The first fs-laser pulse photodetaches the excess electron (**Ne**gative → **Ne**utral) and creates a vibrational wave packet on the electronic ground state of the neutral particle. As a consequence of the Franck-Condon principle, the initial configuration of the neutral molecule is identical with the structure of the negatively charged cluster. This initial configuration of the neutral particle can correspond to a non-equilibrium structure along the

coordinate of a chemical reaction and the system starts to evolve in order to reach the equilibrium structure. After a variable delay time, the second fs-laser pulse ionizes the neutral molecule (**Ne**utral → **Po**sitive) and the signal of the cations is detected as a function of the delay time between the two laser pulses.

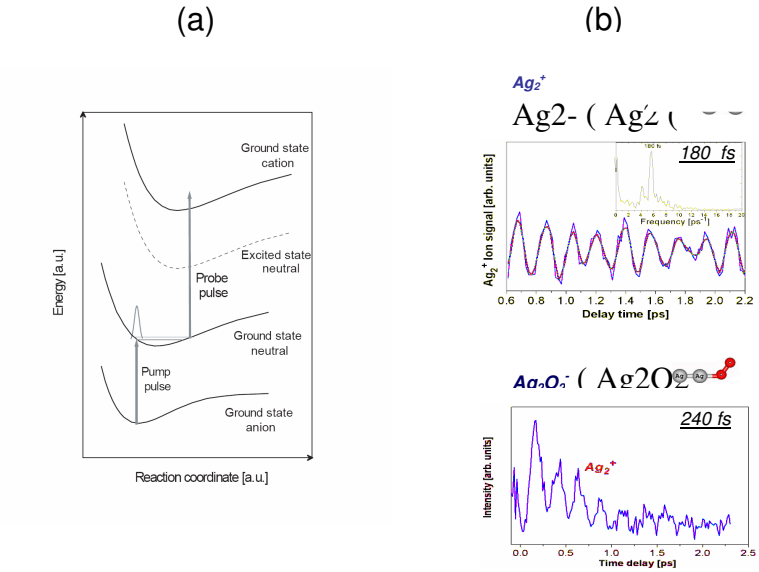

Fig. 4 *(a) Schematic representation of the principle of NeNePo spectroscopy. (b) Experimental NeNePo signal for pure silver dimers (upper part) and* Ag_2^+ *fragment resulting from the neutral* Ag_2O_2 *dissociation after photodetachment of* $Ag_2O_2^-$ *(lower part).*

This experimental scheme was successfully applied in the case of Ag_2 and Ag_2O_2 systems. Fig. 4b (upper part) presents the NeNePo spectrum of Ag_2 recorded in a one-color experiment (406 nm) at 100 K for delay times $t_D > 600$ fs. An oscillation of the neutral silver dimer with a period of 180 fs can be observed. This periodic signal corresponds to an oscillation of the prepared wave packet between on the $X1^1\Sigma_g$ singlet ground state of the neutral silver dimer [10]. When a partial pressure of oxygen is added inside the ion trap, Ag_2^- reacts to yield $Ag_2O_2^-$ within less than 100 ms. Fig. 4b (lower part) shows the results of a NeNePo experiment starting with $Ag_2O_2^-$ reaction species. The measurements are performed at 100 K and the same wavelength of the laser beam (406 nm) is employed as in the case of bare silver dimers. It can be seen that the signal of the Ag_2^+ fragment obtained from the neutral Ag_2O_2 dissociation shows an oscillation with a period of 240 fs. In comparison with the dynamics of bare Ag_2 under similar experimental conditions, the influence of the oxygen adsorbate is found to lead to a considerable energy transfer to the silver dimer governed by a strong vibrational excitation of Ag_2. The results demonstrate the viability of this approach to gain insights into reactive processes of molecular

metal cluster. The future extension of these investigations to larger clusters is expected to open new routes to the understanding of fundamental reaction dynamics on metal clusters.

3. Structure determination: vanadium oxide cations

Vanadium oxides, especially V_2O_5, are known for their catalytic activity in oxidation-reduction reactions [11], as well as other properties e.g. infrared coatings [12], sensors [13] and semiconductors. Many catalysts have vanadium oxide dispersed over different supports. The advantage of supported vanadium oxides lies in the variability of their geometric and electronic structure [11]. Infrared (IR) spectroscopy is a very powerful method for structure determinations. However, conventional absorption measurements lack the sensitivity and selectivity required for the study of isolated gas phase ions, mainly due to the low number densities compared to the solution and condensed phase. The development of free electron lasers with tunable and intense radiation enabled the measurement of infrared spectra of gas phase ions [14]. Infrared photodissociation (IR-PD) spectroscopy is one of the most frequently applied methods. IR-PD using free electron lasers is, however, very inefficient for small systems compared to the large ones, because the transition from the discrete to the quasi-continuum region is shifted to high energies. This bottleneck can be circumvented by using the "messenger atom technique" [15]. This method has the advantage that absorption of only few (mainly one) photons is sufficient to induce photodissociation. $X^+ \cdot He \xrightarrow{h\nu} [X^+ \cdot He]^* \rightarrow X^+ + He$

The IR-PD spectra of polyatomic vanadium oxide cations were recorded using the radiation from the Free Electron Laser for Infrared eXperiments, FELIX [16]. A detailed description of the experimental setup and measurement procedure was published previously [17,18]. The cooled (15K) radio frequency ion trap is filled with ions, which are allowed to thermalize. The weakly bound complexes are formed through three-body collisions with the He buffer gas in the trap. Previous studies [17] have shown that the rare gas atom is benign. IR-PD spectra of vanadium oxide clusters were detected after photo-excitation of the trapped ions with the FELIX radiation, extraction and mass selection. IR photodissociation spectra of trapped $VO_x^+ \cdot He_n$ (x=1-3, n=1,2) and $V_2O_x^+ \cdot He_n$ (x=2-6, n=1-3) cations are shown on the bottom rows of Fig. 3 and 4. Resonant absorption of photons results in a depletion of the complex ion signal and signal increase of the bare ion parent. The photoformation signal of the bare ion from dissociating complexes is small compared to the total bare ion signal, since most of the ions in the trap remain

uncomplexed. Thus, photoabsorption can be detected with higher efficiency in the depletion spectra. The IR-PD spectra of several systems discussed here were measured by monitoring the depletion of the complex with more than one He atoms which gave a better signal to noise ratio. Assuming a sequential formation mechanism, this can be attributed to a faster reformation of the n=1 than of the n=2 or n=3 complexes. The upper rows of Fig. 5 and 6 show the simulated IR absorption spectra based on scaled

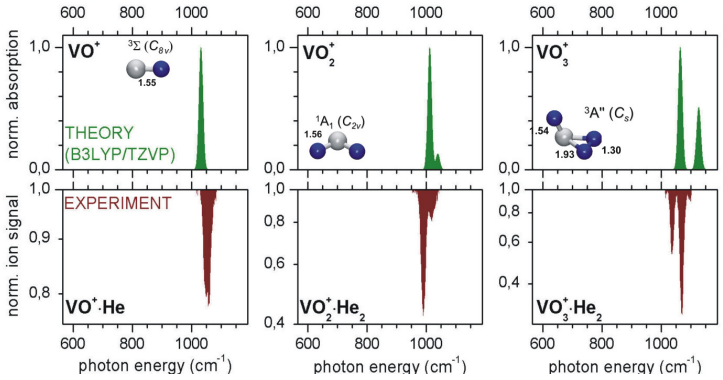

Fig. 5: *IR-PD spectra of VO^+, VO_2^+ and VO_3^+ complexed with one or two He atoms (lower row) in the region between 565 and 1190 cm^{-1}. The upper row shows the simulated IR absorption spectra based on scaled B3LYP/TZVP frequencies and relative intensities of the ground state of VO_x^+ (x=1-3) [17,18].*

B3LYP/TZVP frequencies and relative intensities of the ground states calculated by Sauer et al. [18]. Comparison of the IR-PD spectra for VO_x^+ cations with the simulated ground state spectra indicates a good agreement. All infrared bands lie above 900 cm^{-1}, region characte-ristic for vanadyl stretches. The predicted structures for VO^+ and VO_2^+ show one, respectively two equivalent V-O bonds, whereby the later prefers a bent structure. The full width at half maximum (FWHM) of the IR band in the depletion spectrum of VO^+·He is ~ 27 cm^{-1}, larger than the FELIX bandwidth (9 cm^{-1}). This might be attributed to either additional bands or rotational excitation. Spectra simulations have indicated a mean rotational temperature of 70 K for the ions in the trap [17]. The VO_3^+·He_2 spectrum agrees best with the predicted, scaled vibrational frequencies for an oxovanadium (V) - η^2 – superoxide structure as shown in Fig. 5, right panel. In contrast to the small vanadium oxide clusters discussed above, the larger systems of the type $V_2O_x^+$ (x=2-6) show IR bands below 900 cm^{-1} as well, which are an indication for the presence of a four-membered V-O-V-O ring (see Fig. 6). Six ring vibrational modes are predicted for the ring vibrations, but three of them (ν_{scaled}= 835, 700 and 565 cm^{-1}), which show in-plane deformation modes, are the most intense. These three modes represent the spectroscopic “fingerprint” for the

ring structure [18]. Comparisons of the experimental with the simulated IR spectra for the ground electronic states which have a predicted four-membered V-O-V-O ring structure (Fig. 6), show a reasonable agreement for all systems. In case of $V_2O_2^+$, additional two low lying states with relative energies lower than 10 kJ/mol were found. They show very similar predicted IR spectra making the assignment to the electronic ground state difficult. Larger clusters than $V_2O_2^+$ show additional vanadyl groups to the ring. For $V_2O_4^+$, these may occupy either *trans* or *cis* positions. The experi-mental spectrum agrees best to the *cis* conformer, however the calculations predict the

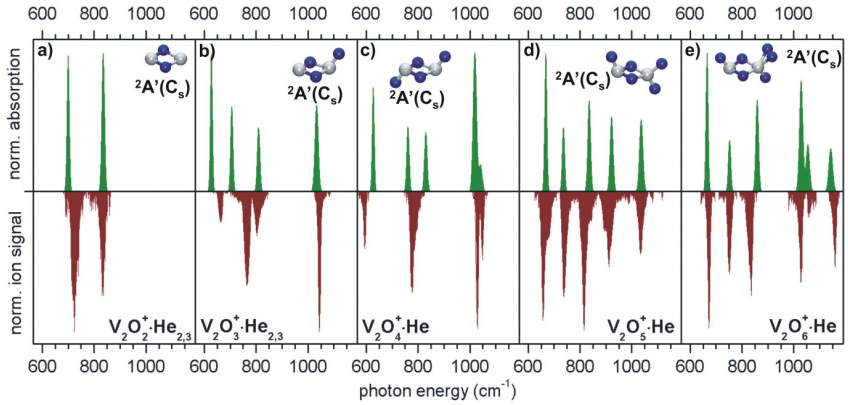

Fig. 6*: Simulated IR absorption spectra based on scaled B3LYP/TZVP frequencies and relative intensities of the ground state (upper row). High resolution experimental IR-PD spectra for $V_2O_2^+$·$He_{2,3}$, $V_2O_3^+He_{2,3}$, $V_2O_4^+$·He, $V_2O_5^+$·He and $V_2O_6^+$·He between 565 and 1190 cm^{-1} are shown in the bottom row [18].*

structure with *trans* orientation of the vanadyl groups as the lowest energy conformer [18]. Additionally, the unpaired d electron may localize on one of the vanadium atoms leading to a distortion of the symmetry along the V–V axis [19]. Thus, the V-O-V-O ring has two larger and two shorter V-O bonds. The highest frequency band in $V_2O_6^+$ spectrum located at 1160 cm^{-1} lies outside the frequency range predicted for vanadyl groups and it is assigned to a superoxo group [18]. Although the presented systems are small compared to the bulk, striking similarities with the properties of a vanadium oxide single-crystal surface were found already for $V_8O_{20}^-$ [20], which thus becomes an interesting gas phase model system to study surface adsorption and reactivity.

5. Coherent control of ultrafast photoinduced reactions

Since Judson and Rabitz [21] proposed the adaptive feedback method for controlling reaction pathways with shaped fs pulses, there was a high interest in the experimental applying

[22–25]. By using an iterative process, the method enables one to find an optimal pulse form, which forces the system into the target state. Usually, the aim of quantum control experiments is to increase the efficiency of photo chemical reactions, but a new major goal of closed loop experiments is to gain information about molecular dynamics and the photo-induced control process itself [26]. Alkaline metal clusters are excellent model systems for coherent control experiments as they exhibit absorption bands located within the operating range of commercial fs-laser sources. In order to optimize the 3-photon ionization process of NaK signal a self-learning algorithm is implemented between ion signal detector and pulse shaper. The basic components of the experimental setup like the supersonic molecular beam apparatus, the quadrupole mass spectrometer, and the fs-laser are described elsewhere [24].

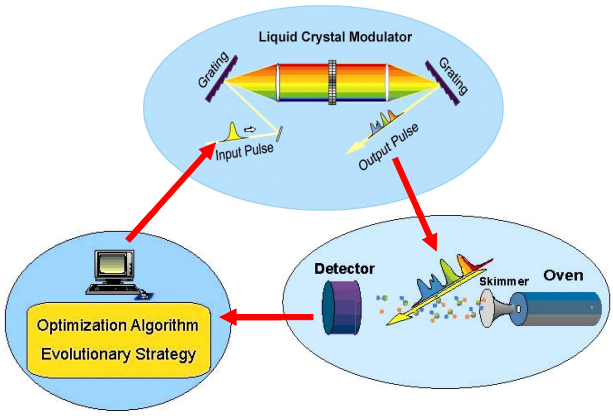

Fig. 7: *Experimental realization of the feedback loop. The optimization algorithm writes patterns onto the liquid crystal window which modulate the fs-puls in phase and amplitude. The shaped pulses are send to the neutral molecular beam and evaluated by the ion signal they produce.*

As shown in Fig. 7, the laser beam is passed across a zero dispersion compressor in a 4f-arrangement, consisting of two gratings and two plano-convex lenses. Simultaneous and independent phase and amplitude modulation is achieved by applying voltages to the double mask liquid crystal spatial light modulator (SLM) consisting of 2 x 128 pixels [27] placed in the Fourier plane of the compressor. The modulated pulses are then focused onto the molecular beam. As feedback signal the ion current of the desired mass-selected cluster is taken. According to this feedback signal an algorithm based on evolutionary strategies iteratively creates and selects pulse forms. Convergence is reached when the feedback signal is maximized and the optimized pulse form is found. Details of the algorithm have been published elsewhere [24]. The optimized pulse shapes are analyzed by intensity and frequency-resolved cross-correlation technique (X-FROG). The optimization of the combined multi-photon ionization and

fragmentation from mixed triatomic alkaline metal clusters is considered. After the convergence of the optimization algorithm, NaK ion signal rises by a factor of 1.8 than the NaK ion signal recorded with an unshaped pulse. The optimized pulse is shown in its cross correlation (Fig. 8a) and time-frequency X-FROG representation (Fig. 8b). It consists of a pulse train composed of three main pulses with a most intense middle pulse. The time delays between the first and second pulse and between the second and third pulse are $\Delta t_{1,2}$ ~ 660 fs and $\Delta t_{2,3}$ ~ 440 fs, respectively. The intensity of the central pulse is about three times higher than the first pulse and twice as high as the third one leading to a sub pulse intensity ratio of 1:3:2. In the X-FROG trace (Fig. 8b) the central pulse reveals a pronounced

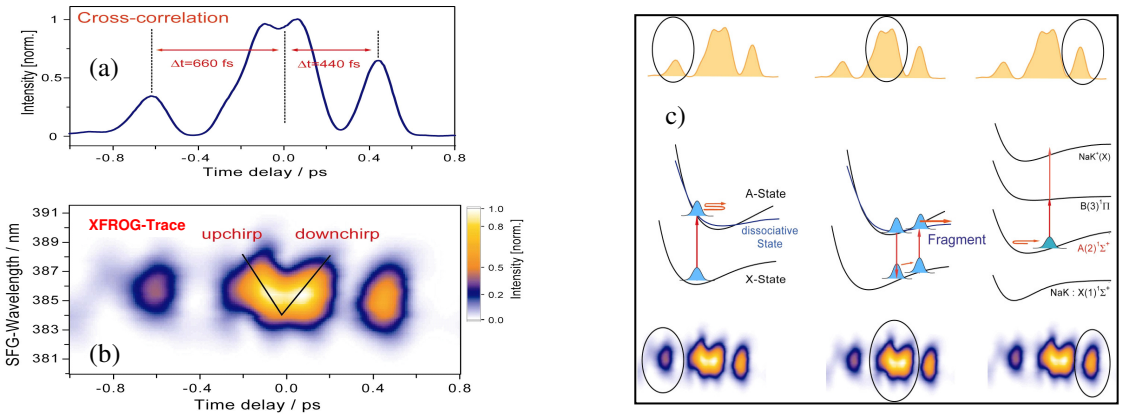

Fig. 8 *Cross-Correlation (a) and its corresponding XFROG (b) traces of the optimal pulses obtained for the dissociation of Na_2K to NaK. (c) Reaction pathway mechanism deciphered from the optimal pulse form.*

positive and negative chirped substructure. On the red side of the spectrum the pulse is divided into two sub pulses ($\Delta t_{2a,2b}$ ~ 150 fs) whose intensity maxima converge in a V-shape showing a positive chirp which is followed by a negative chirp. The structure of the optimized pulse form exhibits features of the NaK dynamics which are similar to the maximization of the NaK ionization [28]. Since the pulse form optimizes both the ionization and the fragmentation processes, the substructure of the central pulse indicates a contribution to the fragmentation of mainly Na_2K into NaK. This substructure can be explained as follows. The first pulse creates a wave packet not only in the $A(2)^1\Sigma^+$ state of NaK but also in the corresponding excited state of the fragmenting trimer (Fig. 8c). The V-shaped substructure of the central pulse (see the XFROG trace in Fig. 8b) can be explained in the following way. The leading red shifted part stimulates the population of the trimer into a vibrationally excited state of the ground state where due to

conservation of momentum the wave packet moves in the same direction. The central part of the second pulse hits the wave packet of the NaK cluster also present in the beam after $\Delta t = 1.5 \times T^{NaK}_{osc}$ and promotes it to an ionic state. The trailing part of the central pulse is again red shifted and therefore able to lift the ground state wave packet of the triatomic molecule located now beyond the curve crossing onto the repulsive potential curve of the trimer. In this way the system avoids the predissociative curve crossing and therefore finds a direct exit channel. Last, the third pulse ionizes the NaK fragments produced from Na_2K. As the last pulse arrives after another full round trip, it can also effectively ionize the remaining wave packet in the non-fragment NaK, since it is again located at the outer turning point of the potential. Thus, also in this case the third pulse improves the ionization efficiency under the constraint of the fragmentation task. The rise in the NaK^+ yield of about 20% compared to the optimization of the pure ionization of NaK [28] corresponds to the gain in NaK^+ determined in the pump–probe spectrum. This leads to the conclusion that the optimized fragmentation into NaK is effective and insights about the control mechanism could be gained from the optimized pulse shape.

6. Conclusion

In this review article we presented several experiments which have contributed to the study of dynamical properties of metal clusters. Reactivity experiments have indicated that gold becomes reactive once the size of the system is reduced. IR spectroscopy, combined with quantum chemical calculations revealed the structural properties of small clusters. The ultrafast dynamics of small molecules were investigated by fs time-resolved spectroscopy. The optimal control technique is able to find a laser pulse which influences a chemical reaction and enhances the desired product yield. A closer look at the optimized pulse shape can reveal mechanistic insights about the chosen reaction pathways.

Acknowledgments:

This work was supported by the Sondersforschungsbereich 450 and 546 of the Deutsche Forschungsgemeinschaft. We gratefully acknowledge all of our, in the references mentioned coworkers and the support of the Stichting voor Fundamenteel Onderzoek der Materie (FOM) in providing the required beam time on FELIX.

References:

[1] Cho, A. Science (2003)**,** 299*,* 1684.
[2] M. Haruta, Catal. Today (1997), 36, 153.
[3] B. C. Gates, Catalytic Chemistry, John Wiley & Sons, Inc.: New York, Singapore, 1992.
[4] A. Sanchez, S. Abbet, U. Heiz, W.-D. Schneider, H. Häkkinen, R. N. Barnett, U. Landmann, J. Phys. Chem. A (1999), 103, 9573.
[5] L.D. Socaciu, J. Hagen, U. Heiz, T. M. Bernhard, T. Leisner, L. Wöste, Chem. Phys. Lett. (2001), 340, 282.
[6] J. Hagen, L. D. Socaciu, M. Elijazyfer, U. Heiz, T. M. Bernhardt, L. Wöste, Phys. Chem. Chem. Phys. (2002), 4, 1707.
[7] J. Hagen, L. D. Socaciu, J. Le Roux, D. Popolan, T. M. Bernhardt, L. Wöste, R. Mitrić, H. Noack, V. Bonačić -Koutecký, J. Am. Chem. Soc. (2004), 126, 3442.
[8] L. D. Socaciu, J. Hagen, T. M. Bernhardt, L. Wöste, U. Heiz, H. Häkkinen, U. Landman, J. Am. Chem. Soc. (2003), 125, 10437.
[9] H. Häkkinen, U. Landman, J. Am. Chem. Soc. (2001), 123, 9704.
[10] L. D. Socaciu-Siebert, J. Hagen, J. Le Roux, D. Popolan, M. Vaida, Š. Vajda, T.M. Bernhardt, L. Wöste, Phys . Chem. Chem. Phys .,(2005) , 7 , 2706; T.M. Bernhard, J. Hagen, L.D. Socaciu, R. Mitrić, A. Heidenreich, J. Le Roux, D. Popolan, M. Vaida, L.Wöste, V. Bonačić-Koutecký, J. Jortner, ChemPhysChem (2005), 6, 243.;
[11] B.M. Weckhuysen and D.E. Keller, Catalysis Today, 78 (2003) 25.
[12] E.E. Chain, Appl. Opt., 30 (1991) 2782.
[13] G. Micocci, A. Serra, A. Tepore, S. Capone, R. Rella, P.J. Siciliano, Vac. Sci. Technol. A, 15 (1997) 34.
[14] H. Piest, G. von Helden, G. Meijer, J. Chem. Phys., 110 (1999) 2010.
[15] M. Okumura, L. I. Yeh, Y. T. Lee, J. Chem. Phys., 83 (1985), 3705
[16] D. Oepts, A. F. G. van der Meer, P. W. van Amersfoort, Inf. Phys. Tech., 36 (1995) 297.
[17] M. Brümmer, C. Kaposta, G. Santambrogio, K. Asmis, J. Chem. Phys., 119, (2003) 12700.
[18] K. R. Asmis, G. Meijer, M. Brümmer, C. Kaposta, G. Santambrogio, L. Wöste, J. Sauer, J. Chem. Phys., 120 (2004) 6461
[19] M. Pykavy, C. van Wüllen, J. Sauer, J. Chem. Phys., 120 (2004) 4207.
[20] K. R. Asmis, G. Santambrogio, M. Brümmer, J. Sauer, Angew. Chem., 44 (2005) 3123.
[21] R.S. Judson, H. Rabitz, Phys. Rev. Lett. 6, (1992),1500
[22] C.J. Bardeen, V.V. Yakovlev, K.R. Wilson, S.D. Carpenter, P.M.Weber, W.S. Warren, Chem. Phys. Lett 280 (1997),151
[23] A. Assion, T. Baumert, M. Bergt, T. Brixner, B. Kiefer, V.Seyfried, M. Strehle, G. Gerber, Science 282 (1998) 919
[24] Š. Vajda, A. Bartelt, C. Kaposta, T. Leisner, C. Lupulescu, S. Minemoto, P. Rosendo Francisco, L. Wöste, Chem. Phys. 267, (2001), 231
[25] A. Lindinger, C. Lupulescu, M. Plewicki, F. Vetter, A. Merli, S. M. Weber, and L. Wöste, Phys. Rev. Lett. 93 (2004), 033001
[26] C. Daniel, J. Full, L. Gonzáles, C. Lupulescu, J. Manz, A. Merli, Š. Vajda, L. Wöste, Science 299, (2003), 536.
[27] A. M. Weiner, D. E. Leaird, J. S. Patel and J. Wullert, IEEE J. Q. Electron., 1992, 28, 908
[28] A. Bartelt, A. Lindinger, C. Lupulescu, Š. Vajda and L. Wöste, Phys. Chem. Chem. Phys., 2004, 6, 1679